

# Solid oxygen as converter for the production of ultra-cold neutrons

A. Frei,<sup>1,\*</sup> F. Böhle,<sup>1</sup> R. Bozhanova,<sup>1</sup> E. Gutschiedl,<sup>1</sup> T. Huber,<sup>1</sup> J. Klenke,<sup>2</sup> S. Paul,<sup>1</sup> and S. Wločka<sup>1</sup>

<sup>1</sup>*Physik Department, Technische Universität München, James-Frank-Str. 1, D-85748 Garching*

<sup>2</sup>*Forschungsneutronenquelle Heinz Maier-Leibnitz (FRM II),  
Technische Universität München, Lichtenbergstr. 1, D-85748 Garching*

We have investigated solid oxygen as a converter material for the production of ultra-cold neutrons. In a first series of experiments the crystal preparation was examined. An optically semi-transparent solid  $\alpha$ -oxygen crystal has been prepared. In a second series of experiments this crystal has been exposed to the cold neutron flux of the MEPHISTO beam line of the FRM II. Ultra-cold neutrons produced inside the oxygen crystal have been extracted and the count rates have been measured at different converter temperatures. The results of these measurements give a clear signal of the superthermal production mechanism due to antiferromagnetic lattice excitations in  $\alpha$ -oxygen. The mean free loss length of UCN inside the crystal was determined to be  $\approx 30$  cm.

PACS numbers: 28.20.Cz, 29.25.Dz, 78.20.-e

Keywords: Ultra-cold neutrons, Solid oxygen converter

Precision experiments with ultra-cold neutrons (UCN), such as the search for a possible electric dipole moment (EDM) of the neutron or the measurement of the lifetime  $\tau_n$  of the free neutron, require high UCN densities. Stronger UCN sources are presently developed [1–9], based on the principle of superthermal UCN production [10, 11] using cryo-converters made of solid deuterium, superfluid helium or solid oxygen. Until now promising results have been achieved with converters made of deuterium or helium. Another very promising candidate is solid oxygen, where UCN can be produced via phonon and magnon excitations in the crystal lattice. It has a large neutron-magnon inelastic scattering cross section and a small nuclear absorption cross section, and offers therefore the possibility to install large (several dm) converters at UCN sources with high ultra-cold neutron production rates. Since oxygen is antiferromagnetic and magnons can be excited only at the  $\alpha$ -phase ( $T < 23.9$  K) a solid oxygen crystal has to be grown, which has to be optically transparent to minimize losses during the extraction of UCN out of the converter.

In solid oxygen at low temperatures the thermal excitations of the lattice freeze out and long range antiferromagnetic ordering is established, leading to a two-dimensional antiferromagnetic structure [12]. In addition to phonon excitations also magnetic spin wave excitations (magnons) contribute to the neutron scattering. This supplementary magnetic scattering of neutrons might be a strong down-conversion channel, which would enhance the production of ultra-cold neutrons. Theoretically this process was considered for the first time by [13]. Experimentally the neutron scattering cross sections and UCN production cross sections of solid  $\alpha$ -oxygen have been investigated by different groups, e.g. [14, 15], concluding that the UCN production rate should increase by cooling down the solid oxygen crystal to temperatures below 20 K. But direct measurements of UCN count rates from such crystals conducted recently could not confirm the

expected results [16, 17]. On the contrary the measured UCN count rates did not increase when lowering the crystal temperature, or even decreased. The reason for this is still unknown and most assumptions hold the losses due to UCN-extraction out of the oxygen crystal responsible for the measured effects.

We report here on a series of measurements, on the one hand investigating the optical properties of an oxygen crystal, and on the other hand measuring the temperature dependence of count rates of UCN produced by an oxygen converter.

Ultra-cold neutrons have energies  $E < 300$  neV, corresponding to De Broglie wavelengths  $\lambda > 50$  nm. Thus the wavelength spectrum of ultra-cold neutrons with the lowest energies covers the spectrum of visible light. Therefore the optical properties of an oxygen crystal are important. Optical transparency of the crystal is a prerequisite to minimize losses occurring during the extraction of UCN out of the crystal.

There are six solid state phases of oxygen known to exist, but only three of them occur at vapor pressure [18]. An overview of the characteristics of these phases is given in Tab. I. With our setup no pressure could be applied to the crystal, so only the  $\alpha$ -,  $\beta$ - and  $\gamma$ -phases occurred during our measurements.

In our experiment the procedure for generating an  $\alpha$ -oxygen crystal is the following: Cooling of the sample cell to  $T \sim 70$  K, liquification of inflowing oxygen gas and further cooling of the sample cell down to  $T \approx 10$  K at vapor pressure conditions. Hereby the transitions liquid  $\rightarrow \gamma$ ,  $\gamma \rightarrow \beta$  and  $\beta \rightarrow \alpha$  occur during the cooling process. Before measuring the UCN production at this different phases the oxygen crystal was optically inspected, and the cooldown rates especially at the phase transitions were optimized. Therefore a sample cell ( $70 \times 70 \times 70$  mm) made of aluminium is connected to a 4K-Cold-Head (type RDK-415D of Sumitomo Heavy Industries ltd.) with a power of 1.5 W at 4 K at its bottom side. The usable

Phase	Color	Pressure	Temperature	Structure	Symmetry
$\alpha$ -phase	light blue	vapor	< 23.9 K	monoclinic	$C2/m$
$\beta$ -phase	blue	vapor	23.9 K – 43.8 K	rhombohedral	$R\bar{3}m$
$\gamma$ -phase	faint blue	vapor	43.8 K – 54.4 K	cubic	$Pm\bar{3}n$
$\delta$ -phase	orange	9.6 GPa – 10 GPa	—	orthorhombic	$Fm\bar{3}m$
$\epsilon$ -phase	red	10 GPa – 96 GPa	—	monoclinic	$A2/m$
$\zeta$ -phase	metallic	> 96 GPa	—	metallic	—

TABLE I: Solid state phases of oxygen [18].

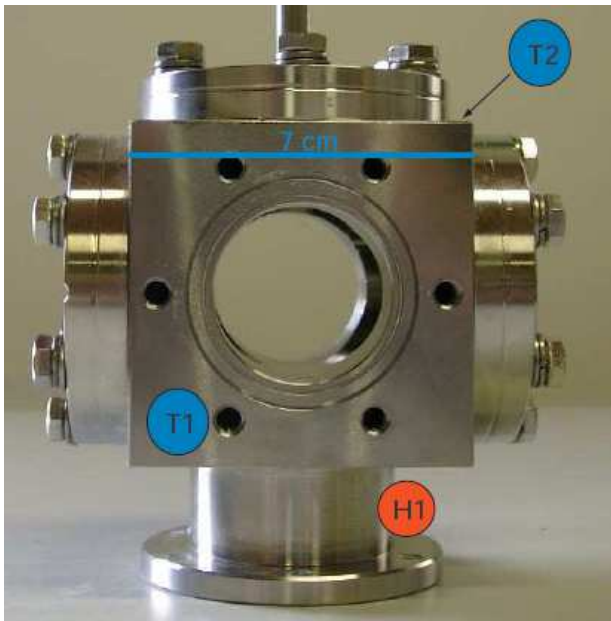


FIG. 1: Sample cell (dismounted) for optical investigation of the oxygen crystal. Material: Aluminium. Down side can be connected to a cold head. H1 shows the position of a 70 W heater. T1 and T2 are the positions of temperature sensors. Gas inlet from top. Not shown: Glass windows on the front and rear side for optical inspection.

volume for the oxygen inside the cell is  $35 \times 35 \times 35$  mm. At the bottom of the cell a 70 W heater is installed to adjust the temperature, which is measured by two temperature sensors (type Cernox CX-1050-AA of LakeShore Cryotronics Inc.) at the bottom and at the top of the cell. As gas inlet a stainless steel tube ( $8 \times 1$  mm) is connected to the top. At the front and rear side two glass windows are mounted to the cell for optical inspection of the oxygen volume. Fig. 1 shows a picture of the sample cell.

In a first series of experiments the cooldown rates especially at the phase transitions were optimized, and the oxygen crystal was optically inspected. At the transition liquid  $\rightarrow \gamma$ , which occurs at 54.4 K at vapor pressure [19], the cooling rate had no influence on the transparency of the resulting  $\gamma$ -crystal. Hereby the cooling rates were varied in the range of  $1.0 - 0.1$  K/h. In any case this

crystal had a faint blue color and was optically transparent.

The  $\gamma \rightarrow \beta$  phase transition is a polymorphic transformation from the cubic  $\gamma$ -phase to the rhombohedral  $\beta$ -phase at a temperature of 43.8 K [20] with a heat of transition of  $\Delta H \approx 742$  J/mol [21] and a volume jump of  $\Delta V \approx 1.08$  cm<sup>3</sup>/mol [22]. Due to these circumstances this transition is critical concerning the optical transparency of the resulting  $\beta$ -crystal. In our experiments we found that only at cooling rates of below 10 mK/h the resulting  $\beta$ -crystal was optically cloudy with a blue color. At faster cooling rates the resulting  $\beta$ -crystal was completely black and optically opaque.

The  $\beta \rightarrow \alpha$  phase transition occurs at a temperature of 23.9 K [18]. Questions like this transition being of second order or not, on heat of transition or a volume jump is under dispute. While a heat of transition and a volume jump were measured by several groups [23–26], these results have been questioned by several other groups [21, 27]. In our experiment the cooling rate was varied in the range of  $1.0 - 0.1$  K/h and had no influence on the optical properties of the resulting  $\alpha$ -phase crystal, which showed the same color and transparency as the  $\beta$ -crystal. In Fig. 2 pictures of the different crystals described above can be seen.

In a second series of experiments the sample cell was placed in the cold neutron beam line MEPHISTO of the "Forschungsneutronenquelle Heinz Maier-Leibnitz" (FRM II), and exposed to a cold neutron flux of  $\Phi = 5.25 \cdot 10^9$  cm<sup>-2</sup>s<sup>-1</sup>. The energy distribution of the cold neutrons has almost Maxwellian shape, with a characteristic temperature of  $T = 40$  K. The glass windows of the sample cell were replaced by thin aluminium windows (thickness 500  $\mu$ m, diameter 35 mm) to allow transparency of incoming and outgoing neutrons. UCN produced were extracted horizontally and perpendicular to the incoming beam through an aluminium window (thickness 200  $\mu$ m, diameter 35 mm) and guided through an electropolished stainless steel tube (inner diameter 66 mm, total length  $\sim 3$  m) to an UCN detector of the CASCADE type [28]. The UCN extraction tube was bent by 90° in the horizontal plane 50 cm away from the sample cell, then had a straight section of 2 m, and was bent again by 90° vertically downwards towards the detector. As an option a



FIG. 2: Pictures of the oxygen crystal at different phases. Top left: Liquid oxygen in the sample cell (partially filled). Top right: Transparent  $\gamma$ -oxygen (sample cell completely filled). Bottom left: Cloudy  $\beta$ -oxygen. Bottom right: Cloudy  $\alpha$ -oxygen.

stainless steel foil (thickness  $100\ \mu\text{m}$ ) could be inserted into the UCN extraction tube. By this only neutrons with energies  $> 190\ \text{neV}$  (corresponding to the Fermi-Potential of the foil material [29, 30]) can penetrate the foil and are counted in the detector, while all UCN with energies  $< 190\ \text{neV}$  are reflected from the foil and don't reach the detector. By subtracting count rates of measurements with the inserted foil (corrected for absorption of neutrons in the foil) from count rates without foil, the effective UCN count rate with UCN energies  $< 190\ \text{neV}$  can be obtained.

In Fig. 3 the resulting UCN countrates measured at different temperatures of the oxygen converter are depicted. The UCN count rate increases with decreasing temperature. This trend is a clear indication of the theoretically expected UCN production and extraction mechanism via the superthermal principle of detailed balance. For a symmetric, monoatomic crystal the double differential neutron scattering cross section for excitation and absorption of a lattice excitation using the incoherent approximation [31] is

$$\frac{d^2\sigma_{\text{inc}}}{d\Omega dE} = a_{\text{inc}}^2 \frac{k_f}{k_i} \kappa^2 \frac{h^2}{2M} e^{-\gamma\kappa^2} \frac{g(|\varepsilon|)}{\varepsilon (1 - e^{-\varepsilon/k_B T})}. \quad (1)$$

Hereby  $a_{\text{inc}}$  denotes the scattering length,  $\kappa = k_f - k_i$  the difference of the final and initial state wavenumber,  $h$  Planck's constant,  $M$  the mass of the scattering atom in units of the neutron mass,  $\varepsilon = E_i - E_f$  the difference

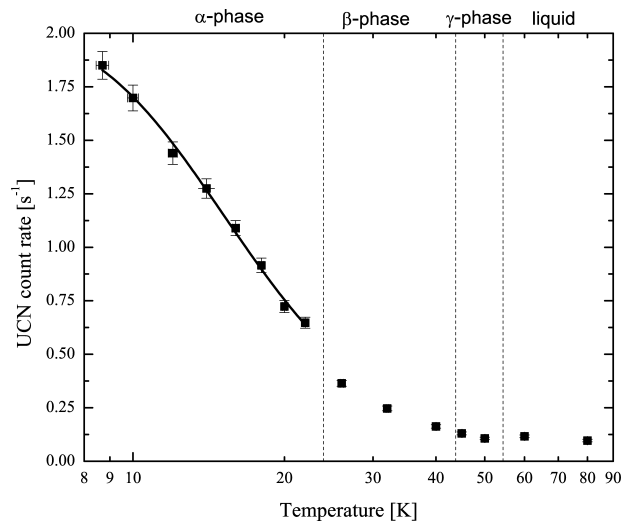


FIG. 3: Filled squares: Measured UCN count rates produced by a solid oxygen converter, depending on its temperature and solid state phase. Error bars include statistical uncertainties and variations in the detector efficiency due to different UCN energies. Solid line: Fit of theoretically expected curve according to Eq. 5

of the initial and the final neutron energy,  $g(|\varepsilon|)$  the generalised density of states,  $\gamma$  the Debye-Waller factor and  $k_B$  Boltzmann's constant. The temperature dependence of the scattering length, the Debye-Waller factor and the density of states in the range from  $8\ \text{K} - 24\ \text{K}$  ( $\alpha$ -oxygen) gives a variation of only about 10% and will therefore be neglected in the following discussion. Thus, the only temperature dependent term left is

$$\sigma_{\text{inc}}(T) \propto \frac{1}{\varepsilon (1 - e^{-\varepsilon/k_B T})}. \quad (2)$$

The UCN production cross section (generation of a lattice excitation,  $\varepsilon = E_i - E_f \approx E_i = 40\ \text{K} \cdot k_B$ ) is temperature independent, since  $e^{-\varepsilon/k_B T} \ll 1$  for  $T < 24\ \text{K}$ . In turn the UCN upscattering cross section (absorption of a lattice excitation,  $\varepsilon < 0$ ) has a temperature dependence (for  $e^{|\varepsilon|/k_B T} \gg 1$ )

$$\sigma_{\text{up}}(T) \propto \frac{1}{|\varepsilon| (e^{|\varepsilon|/k_B T} - 1)} \propto e^{-|\varepsilon|/k_B T}. \quad (3)$$

Thus for constant UCN production rate independent of the crystal temperature, the UCN flux to the detector is proportional to the escape probability  $P_{\text{esc}}$  of UCN leaving the converter,

$$P_{\text{esc}} \propto e^{-N\ell\sigma_{\text{up}}(T)} = e^{-N\ell\sigma_0 e^{-E/k_B T}}, \quad (4)$$

where  $N = 2.9 \cdot 10^{22}$  [32] is the particle density of the converter and  $\ell$  the mean geometrical path of the UCN inside the crystal. Therefore the UCN count rate  $I(T)$

measured at the detector, as seen in Fig. 3, should show a temperature dependence according to

$$I(T) = I_0 e^{-\delta e^{-T_{\text{eff}}/T}}. \quad (5)$$

In Fig. 3 this function has been fitted to the data points measured at  $\alpha$ -oxygen temperatures with  $I_0$ ,  $\delta$  and  $T_{\text{eff}}$  as fit parameters, resulting in  $T_{\text{eff}} = (35 \pm 4)$  K,  $I_0 = (2.0 \pm 0.1) \text{ s}^{-1}$  and  $\delta = 5.6 \pm 0.8$ . From these fit parameters with  $\delta = N\ell\sigma_0$  and  $\sigma(T) = \sigma_0 e^{-T_{\text{eff}}/T}$  one can deduce the mean free loss length  $\lambda(T)$ , assuming that the mean UCN path inside the converter is  $\ell \approx 2$  cm (due to geometry)

$$\lambda(T) = \frac{1}{N\sigma(T)} = \frac{\ell}{\delta e^{-T_{\text{eff}}/T}} \approx 0.36 \cdot e^{35/T[\text{K}]} [\text{cm}]. \quad (6)$$

For  $T = 8$  K the mean free loss path is  $\lambda \approx 30$  cm, which determines the usable size of an  $\alpha$ -oxygen converter. This value is one order of magnitude smaller as compared to the mean free path due to nuclear absorption [13], which means that UCN upscattering, apart from scattering on crystal defects, is the leading loss mechanism limiting the usable converter volume. Another interesting result is the effective temperature of the lattice excitation of  $T_{\text{eff}} = (35 \pm 4)$  K, corresponding to an energy of  $E = k_B T_{\text{eff}} = (3.0 \pm 0.4)$  meV. This result is in agreement with a well known low energy antiferromagnetic excitation at  $\omega/2\pi c = 27 \text{ cm}^{-1}$  or  $E = 3.3$  meV respectively in  $\alpha$ -oxygen [33, 34].

In summary, we have developed a procedure to produce an optically semi-transparent solid oxygen crystal in its  $\alpha$ -phase, which is a prerequisite to minimize extraction losses of UCN out of the crystal. The solid oxygen converter has been exposed to a cold neutron beam, and the UCN count rates have been measured. The measured temperature dependence of the UCN count rate is in agreement with theoretical predictions of the UCN production mechanism due to antiferromagnetic lattice excitations. The usable converter size was determined to be  $\approx 30$  cm. We therefore proofed for the first time experimentally, that solid oxygen is a suitable converter material for UCN production.

This work was supported by the cluster of excellence "Origin and Structure of the Universe" (Exc 153) and by the Maier-Leibnitz-Laboratorium (MLL) of the Ludwig-Maximilians-Universität (LMU) and the Technische Universität München (TUM). We thank T. Deuschle and H. Ruhland for their help during the experiments.

---

\* Corresponding author: Andreas.Frei@ph.tum.de

- [1] U. Trinks, F.J. Hartmann, S. Paul, W. Schott, Nucl. Instrum. Methods A **440**, 666 (2000).  
 [2] Y. Masuda et al., Phys. Rev. Lett. **89**, 284801 (2002).  
 [3] C.A. Baker et al., Phys. Lett. A **308**, 67 (2003).  
 [4] A. Saunders et al., Phys. Lett. B **593**, 55 (2004).

- [5] A. Frei et al., Eur. Phys. J. A **34**, 119 (2007).  
 [6] E. Korobkina, B.W. Wehring, A.I. Hawari, A.R. Young, P.R. Huffman, R. Golub, Y. Xu, and G. Palmquist, Nucl. Instrum. Methods A **579**, 530 (2007).  
 [7] O. Zimmer, K. Baumann, M. Fertl, B. Franke, S. Mironov, C. Plonka, D. Rich, P. Schmidt-Wellenburg, H.-F. Wirth, and B. van den Brandt, Phys. Rev. Lett. **99**, 104801 (2007).  
 [8] A. Anghel et al., Nucl. Instrum. Methods A **611**, 272 (2009).  
 [9] A.P. Serebrov et al., arXiv:0808:3978v3 (2009).  
 [10] R. Golub and J.M. Pendlebury, Phys. Lett. A **53**, 133 (1975).  
 [11] R. Golub, C. Jewell, P. Ageron, W. Mampe, B. Heckel, and I. Kilvington, Z. Phys. B **51**, 187 (1983).  
 [12] P.W. Stephens and C.F. Majkrzak, Phys. Rev. B **33**, 1 (1986).  
 [13] C.-Y. Liu and A.R. Young, arXiv:nucl-th/0406004v1 (2004).  
 [14] F. Atchison et al., Nucl. Instrum. Methods A **611**, 252 (2009).  
 [15] A. Frei, F. Böhle, E. Gutschiedl, A. Maier, S. Paul, H. Schober, and A. Orecchini, arXiv:0911.4398v1 [nucl-ex] (2009).  
 [16] D. Salvat et al., *UCN production in oxygen: Experimental results*, 7th International UCN Workshop, St. Petersburg, Russia 2009 (unpublished).  
 [17] F. Atchison et al., *Production of ultracold neutrons from cryogenic  $^2\text{H}_2$ ,  $\text{O}_2$ , and  $\text{C}^2\text{H}_4$  converters*, handed in for publication to Phys. Rev. Lett. (2010).  
 [18] Yu.A. Freiman and H.J. Jodl, Physics Reports **401**, 1 (2004).  
 [19] D.A. Young, C.-S. Zha, R. Boehler, J. Yen, M. Nicol, A.S. Zinn, D. Schiferl, S. Kinkead, R.C. Hanson, and D.A. Pinnick, Phys. Rev. B **35**, 5353 (1987).  
 [20] J.A. Cowan, R.C. Kemp, and W.R.G. Kemp, Metrologia **12**, 87 (1976).  
 [21] C.-H. Fagerstroem and A.C. Hollis Hallett, J. Low Temp. Phys. **1**, 3 (1969).  
 [22] J.A. Jahnke, J. Chem. Phys. **47**, 336 (1967).  
 [23] A. Eucken, Verhandl. Deut. Physik Ges. **18**, 4 (1916).  
 [24] K. Clusius, Z. Phys. Chem. B **3**, 41 (1929).  
 [25] W.F. Giaque and H.L. Johnston, J. Amer. Chem. Soc. **51**, 2300 (1929).  
 [26] J. Ancsin, Temperature measurements, in: B.F. Billingham, T.J. Quinn, Conference Series No. 26, The Institute of Physics, London and Bristol, 1975, pp. 57–64.  
 [27] R. Muijlwijk, M. Durieux, and H. van Dijk, Physica **43**, 475 (1969).  
 [28] M. Klein, H. Abele, D. Fiolka, and Chr.J. Schmidt, AIP Conf. Proc. **596**, 193 (2001).  
 [29] V.K. Ignatovich, *The Physics of Ultracold Neutrons* (Oxford Science Publications, Clarendon Press, Oxford, 1990).  
 [30] R. Golub, D.J. Richardson, S.K. Lamoreaux, *Ultra-Cold Neutrons* (Adam Hilger, Bristol, 1991).  
 [31] V.F. Turchin, *Slow Neutrons* (Israel Program for Scientific Translations, Jerusalem, 1965).  
 [32] H.M. Roder, J. Phys. Chem. Ref. Data **7**, 949 (1978).  
 [33] T.G. Blocker, M.A. Kinch, and F.G. West, Phys. Rev. Lett. **22**, 853 (1969).  
 [34] R.J. Meier, J.H.P. Colpa, and H. Sigg, J. Phys. C **17**, 4501 (1984).